Research on Engineering Structures & Materials

journal homepage: http://www.jresm.org

Research Group

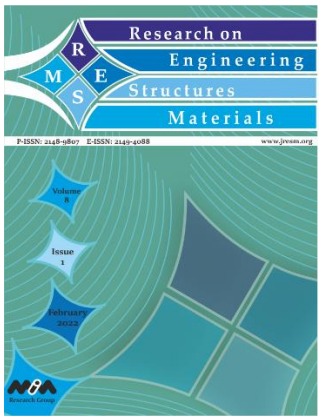

Analysis of various flow field designs for PEM fuel cells used in vehicular systems through 3D modelling

Muhammed Mücahid Toprak, Ceyda Kök, Suha Orçun Mert

Online Publication Date: 27 Oct 2021
URL: http://www.jresm.org/archive/resm2021.328en0805.html
DOI: http://dx.doi.org/10.17515/resm2021.328en0805

Journal Abbreviation: *Res. Eng. Struct. Mater.*

To cite this article

Toprak MM, Kok C, Mert SO. Analysis of various flow field designs for PEM fuel cells used in vehicular systems through 3D modelling. *Res. Eng. Struct. Mater*., 2022; 8(1): 179-203.

Research on Engineering Structures & Materials
journal homepage: http://www.jresm.org
Research Group

Research Article

Analysis of various flow field designs for PEM fuel cells used in vehicular systems through 3D modelling

Muhammed Mücahid Toprak[*1,a], Ceyda Kök[2,b], Suha Orçun Mert[3,c],

[1]*Yuzuncu Yıl University, Department of Chemical Engineering 65080, Kampus, Van, Turkey*
[2]*Iskenderun Technical University- ISTE, Institute of Graduate Studies, 31200 Iskenderun, Hatay, Turkey*
[3]*Iskenderun Technical University- ISTE, Department of Petroleum and Natural Gas Engineering, 31200 Iskenderun, Hatay, Turkey*

Article Info

Article history:
Received 05 Aug 2021
Revised 04 Oct 2021
Accepted 14 Oct 2021

Keywords:

Proton Exchange Membrane;
Fuel Cell;
Electric vehicles;
Modeling and Simulation;
Flow Channels;
CFD

Abstract

The importance of green energy has increased in recent years. Vehicles that don't run on fossil fuels and have zero CO_2 emissions are on the agenda of many developed countries. Battery-based vehicles have long charge times and low range problems, making hydrogen-based fuel cell vehicles a good alternative candidate as a solution. Fuel cell system designs used in these vehicles is one of the most important subjects in the dawn of the renewable energy age. The present study compares different flow channel pattern designs for PEM fuel cells used in vehicles, all of which were designed and modeled as part of the study. Simulations were run on the three-dimensional flow channel designs to determine the most efficient patterns. Efficiency analyses were extended to include the membrane surfaces, where different properties of fuel flow channels, overall energy efficiency, and certain other parameters used in the PEM fuel cell systems were investigated. The study also includes comparison of the designed systems with fuel cell designs currently in commercial use. Finally, the effects of H_2 and O_2 concentrations used in the system were also investigated.

1. Introduction

Energy is a factor that affects the transportation, economy and infrastructure of all developed and developing countries, which in turn greatly influence the living standards of their citizens. The amount of energy required to sustain our civilization is gradually increasing, hand to hand with the technological developments. This energy, however, is mostly supplied through consumption of fossil fuels, which are not sustainable energy sources. Moreover, the rapid depletion of non-renewable energy sources seems to be unstoppable. For this reason, the issue of energy production from renewable energy sources is discussed at international scales by both industrial and scientific communities.

Almost the all of transportation sector uses fossil fuels. Energy Information Administration (EIA) 2014 report shows that 55% of total energy consumption in the world and 30.9% of carbon dioxide gas emissions are in the transportation sector [1]. Figure 1 seems that the CO_2 emissions of the transportation sector in 1990-2015. CO_2 emissions increased from 3.3 gigatonnes (Gt) to 6 Gt for twenty-five years and increased almost 68%.

[*]Corresponding author: orcun.mert@iste.edu.tr
[a] orcid.org/0000-0002-2409-7260; [b] orcid.org/0000-0002-5536-3488; [c] orcid.org/0000-0002-7721-1629
DOI: http://dx.doi.org/10.17515/resm2021.328en0805

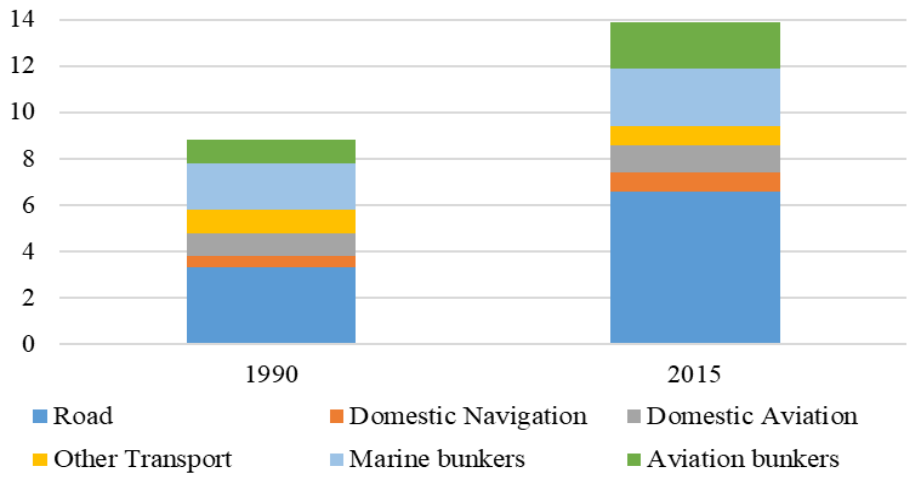

Fig. 1 CO_2 emissions of the transportation sector in 1990-2015 [2]

Interest in new, innovative and green energy sources has increased further in recent years due to the decrease in the amount of non-renewable energy resources. The living standards of developed and developing countries are on a steady increase, which usually is reflected as increased energy demands. There are also environmental concerns with the use of non-renewable energy sources. These developments have placed environmentally-friendly vehicles that do not run on fossil fuels on the agenda of many countries. Scientists have developed and proposed Electric and Hybrid Electric Vehicles (EV's and HEV's, respectively) to alleviate these problems. Lithium Ion (Li-ion) batteries which are used in these vehicles have many advantages such as long shelf life, wide working range, high power and energy density. Yet they also have certain disadvantages such as long charging times and low average ranges. As an alternative to these vehicles, fuel cell vehicles that can store energy in shorter times and offer have a longer range compared to other vehicles have been proposed. It is envisaged that hydrogen can overcome the disadvantages of other vehicles and is a prime candidate as the transportation fuel of the future [3].

There are many reasons to use hydrogen in fuel cell vehicles. The primary advantage of hydrogen lies in its molecular structure, as hydrogen has the simplest form of all molecules. While its energy content per unit volume is relatively low, its energy content per unit weight is the highest amongst all molecules. Unlike fossil fuels, it creates zero emissions when used [4]. Due to these features it has been used in different types of fuel cells and to fuel different types of rockets.

A fuel cell can convert the chemical energy stored in the fuel into electrical energy with a very efficient process that can reach efficiency values as high as 80%. In addition, fuel cells do not emit CO_2 during this process and instead release only water as a by-product. Fuel cells that do not use fossil fuels and do not create emissions are considered environmentally friendly.

Numerous studies have been performed on fuel cells, which lead to improvements in hydrogen applications in the transportation sector. Leading car manufacturers in the industry are now producing fuel cell vehicles, which are mainly available in North America, Asia and Europe. As of June 2018, more than 6500 fuel cell vehicles are reportedly sold. California has the world's largest hydrogen fuel station network, and is a leader in

hydrogen based vehicles where the country delivers 3000 of the 5233 vehicles produced worldwide [5].

Both electric vehicles and fuel cell vehicles have zero CO_2 emissions, and both types of vehicles are environmentally friendly as they use renewable and sustainable energy sources as fuel. The main difference between the two, however, is in refueling and driving distance aspects. Fuel cell vehicles can refuel in less than 10 minutes and offer a driving range of 300 miles on average. It is believed that these vehicles will begin compete in these aspects with conventional fossil fuel vehicles after 2030 [4]. The long-term powertrain scenario is given in Figure 2. According to the figure, International Energy Agency (IEA) estimates that by 2050, the market share of fuel cell vehicles will be 17% with an annual sales of 35 million.

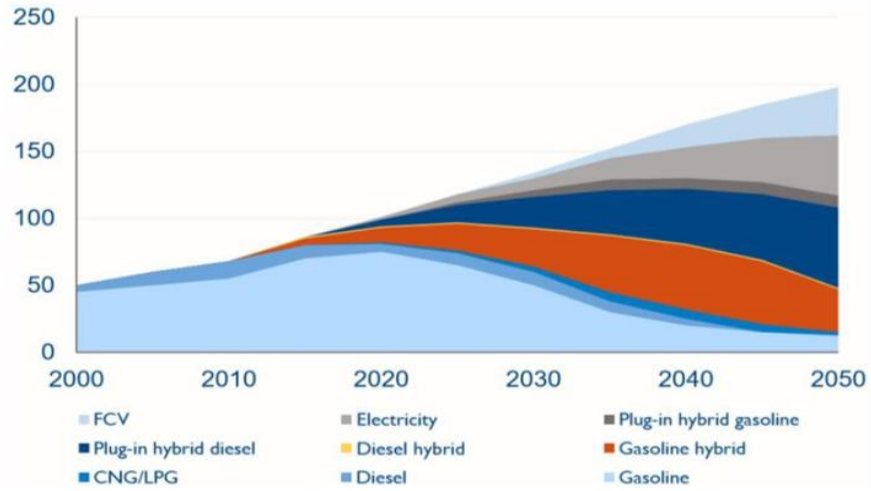

Fig. 2 The long-term scenario of sales [6]

Proton Exchange Membrane (PEM) fuel cell is preferred in fuel cell vehicles that are considered as vehicles of the future. A PEM fuel cell consists of electrodes, flow plates and current collectors. Increasing the fuel cell efficiency and reducing the production costs will make vehicles that use PEM cells preferable. That being said, increasing the efficiency and ensuring a homogeneous reaction rate on the entirety of the catalyst area can only be achieved with the optimum distribution of temperature, concentration, and humidity. This, in turn, can only be achieved by ensuring a homogeneous distribution in the flow plates.

The effect of the flow-field design on PEM fuel battery performance is in the literature. Manso et al. have studied parameters of the types of flow fields, such as width, depth, height, and so on. They also observed the effect of the non-uniform distribution of gases and water on performance. [7]. In flow-field designs, the performance impact of the non-uniform distribution of pressure drop and current density was examined by Fahim et al. [8]. The effects of conventional, serpentine and pin type channel configuration on cell performance were investigated by Pal et al. [9]. Vijay examined the design of serpantin and parallel Z-type flow channel geometry on PEM fuel battery cell performance using CFD modeling simulation [10]. Using the CFD program, the PEM fuel cell with single, double and triple serpentine flow channels and a round-angle active area was designed by Velisela et al. [11]. Shen et al. investigated the performance in the PEM fuel cell by designing parallel, single serpentine and pressurized parallel flow fields to provide a more uniform gas and water distribution [12]. Optimized 3D flow channels have been developed to provide

better flow and mass transfer in the channels [13]. To examine the performance effect of flow channels in a PEM fuel cell, the lung and leaf branches were designed by Badduri et al. [14]. Liao et al. have designed zigzag and straight flow channels for uniform distribution in the PEM fuel cell and examined in terms of their performance [15].

In the present study, six different three-dimensional flow channels were designed with the Comsol multiphysics program, which uses the finite element method for PEM fuel cell. The efficiency analysis of the designed flow channels on the membrane surfaces was made. Energy efficiency of existing designs and proposed designs were compared. This study brings a detailed and comprehensive inner look to the various fuel cell flow field designs that are either currently being used or have the potential to be used in the future for transportation applications. The verified model [16] and simulation covers the concentrations for both of the hydrogen and oxygen inputs, as well as the water content that would flow through the channels and fuel cell, resulting in specific designs. Investigation of the "current density" in different slices was also performed, providing an important perspective for the researchers interested in this property.

2. Fuel Cell

Fuel cells are in essence systems where an electrochemical reaction taking place between an oxidant and a suitable fuel produces electrical energy. These are, therefore, systems that convert the stored chemical energy inside the fuel into electrical energy. This conversion is a result of an reaction that can best be described as the opposite of an electrolysis reaction, and a fuel cell system produces Direct Current (DC) as a result of it. In that regard fuel cells are quite similar to ordinary batteries and accumulators, as they also produce electricity out of an electrochemical process through an electrochemical reaction. The difference, however, lies in the fact that batteries and accumulators are limited with the initial energy stored in them [17], [18], while fuel cells can perform the reaction continuously and infinitely on the condition that they are supplied further fuel and air [19].

Fuel cells are divided into 6 different groups based on their operating temperatures and chemical properties. These are: the Proton Exchange Membrane / Polymer Electrolyte Membrane Fuel Cell (PEMFC), Alkaline Fuel Cell (AFC), Phosphoric Acid Fuel Cell (PAFC), Molten Carbonate Fuel Cell (MCFC), Solid Oxide Fuel Cell (SOFC), and Direct Methanol Fuel Cell (DMFC). Figure 3 shows the areas where these fuel cells are used according to their operating temperatures and power characteristics.

Based on their operating temperatures and power levels, DMFC, AFC, PAFC and PEMFC are considered "low temperature fuel cells", and are generally used in mobile phones, electronic tablets, and transportation. SOFC and MCFC are used in constant power generation and Combined Heat and Power (CHP) applications, as they are high temperature fuel cells and with high power levels.

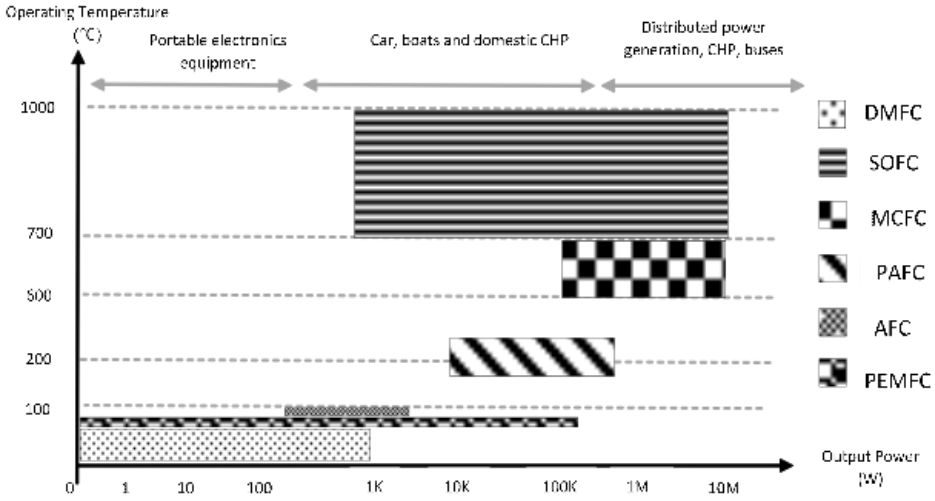

Fig. 3 Fuel cell types according to the operating temperature and power range (adapted) [20].

2.1. Proton Exchange Membrane Fuel Cell

A "Proton Exchange Membrane Fuel Cell" (PEM) is one of the most well thought-out fuel cell designs in terms operational variables. PEM fuel cells have a solid polymer electrolyte membrane which is placed between platinum-catalyzed electrolytes that are porous in structure. This setup provides it with more power density compared to other fuel cells, while reducing its physical volume and weight. The proton-permeable polymer membrane used in PEM cells as the electrolyte is also thinner in structure, where the thickness is measured in micron levels.

PEM cells have quite approachable operational temperatures that are almost always below 100 °C, generally at a ballpark between 60 °C and 80 °C. These cells also use a noble metal –often platinum- as the catalyst, which is quite an advantage in terms of operational properties but increases the production cost. Another disadvantage is the requirement of separation of carbon dioxide from the fuel input, as the platinum catalyst is quite sensitive to it. The separation process also increases the production and operational costs associated with the PEM cells. Different designs suggest the use of platinum/ruthenium catalysts to overcome these shortcomings as this combination is much more durable against carbon monoxide.

The equations provided below show the PEM fuel cell reactions taking place during each cycle: [21]

- Anode Reaction: $2H_2 \rightarrow 4H^+ + 4e^-$
- Cathode Reaction: $4H^+ + 4e^- + ½\ O_2 \rightarrow 2H_2O$
- Total Reaction: $2H_2 + O_2 \rightarrow 2H_2O$ + Electric energy

The working principle of PEMFC fuel cell is given in Figure 4.

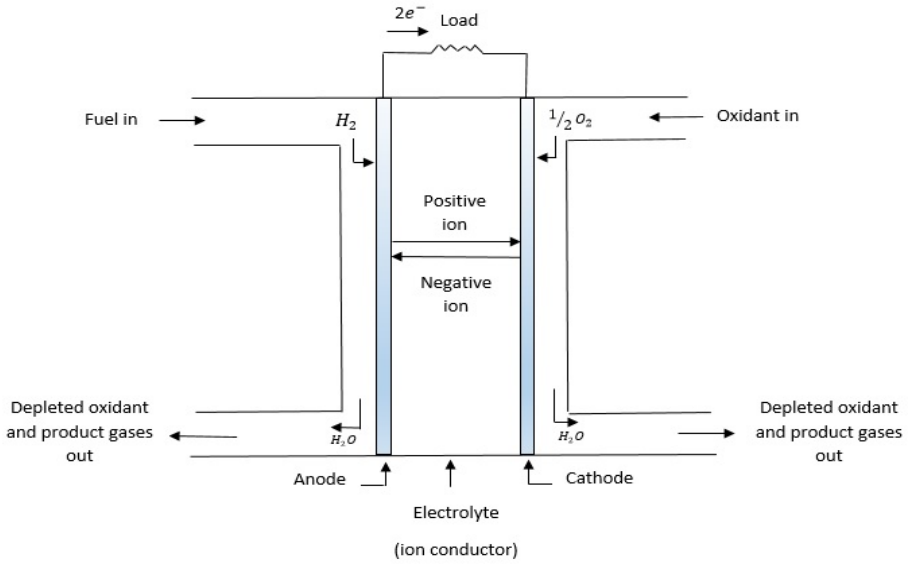

Fig. 4 The working principle of PEMFC fuel cell (adapted) [22]

As can be seen in Figure 4 this fuel cell consists of an anode, a cathode and the electrode. In this design pure hydrogen is used as the fuel, which is fed into the anode. Air (or based on the design, pure oxygen) on the other hand, is fed through the cathode. As the gas passes through the electrolyte membrane on the anode, it decomposes into its electrons. The membrane acts as a filter that separate electrons and hydrogen ions in this process, allowing only the hydrogen ions to pass. The hydrogen ions then combine with oxygen in the cathode compartment to form water molecules (H_2O), through which the reaction heat is released. While in internal combustion engines air and fuel get mixed, in the fuel cell the fuel and the oxidant are separated from each other. Due to this simple difference of operation, fuel cells produce no harmful emissions as internal combustion engines do [23]. This is one of the main reasons why they are preferred in environmentally friendly vehicle designs.

Although there are various types of fuel cells, PEMFC is the most type suitable for vehicles according to scientific works. The fuel cells used an electric vehicle replace the internal combustion engines. Hybrid vehicles that can compete with both electric and conventional vehicles are designed through using PEMFCs with rechargeable batteries. Figure 5 shows the basic design of a fuel-cell electric vehicle.

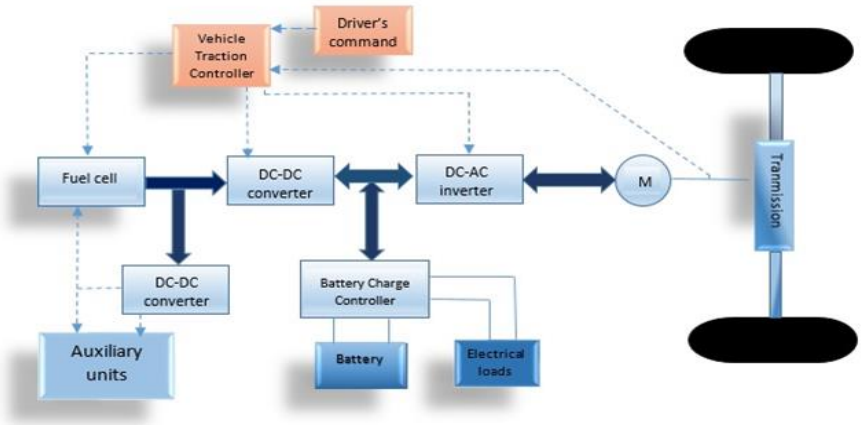

Fig. 5 The basic structure of fuel cell electric vehicles (adapted) [24]

2.2. Performance of the Fuel Cell

The performance of a given fuel cell is based on the performances the performance of the systems that make it up. The performance is primarily tied to the reaction that takes place on the catalyst. The collection of electrons that create the current, the transfer of the hydrogen ions through membrane, and the production of the water as a final product of the combustion reaction all factor into the performance. Finally, the electrical resistances of the components used within the fuel cell also contribute to the performance.

The system of a PEM cell is rather complex and consists of the interactions between numerous chemical and thermodynamic processes. This results in a final performance of the fuel cell that is closely tied to the operating conditions. The most influential operating conditions that influence the fuel cell performance are listed below:

- Temperature
- Pressure
- Membrane thickness
- Humidity
- Current Density

It is important to ensure that the reaction taking place on the catalyst surface is uniform to reach the optimum performance levels. This uniformity is dependent on numerous different parameters the temperature, humidity, and reactant concentration throughout the flow plates. Considering this, 3D models of the investigated flow plate charts were created, and the reactions were simulated to search for the more effective distribution patterns. The results of these simulations were then interpreted to measure the expected performance of different fuel cell designs under different environmental parameters like temperature, concentrations, and humidity.

3. Materials and Methods

3.1. Comsol Multiphysics Simulations

Multiphysics software, which includes a multi-physics infrastructure to run different simulations on the modeled equipment for engineering purposes [25]. The software runs simulations that provide relatively quick results due to having different physical interfaces

being already pre-modeled in it, which cover fluid-flow, electromagnetism, and structural mechanics equations [26]. These pre-defined interfaces that come with the software make it a functional tool to use in solution of different mainstream problems.

The software also has a series of modules that can run near real-like simulations with finite element method simulations. Comsol Multiphysics can model any geometry using different types of materials that can be selected from a built-in library that contains different parameters required to simulate systems that use them. The users can also model their own materials in terms of relative functions. It is possible to work on a single physical geometry, or to simulate numerous geometries that interact with each other in one or more problem steps. Once the system is meticulously modeled using these existing libraries or user entries, simulations can be run to reach multiple potential results or solutions when needed [27].

3.2. Models for the Thermodynamics and Electrochemical Properties of Fuel Cells

Evaluation of the fuel cell performance and analysis of factors that influence it are based on the laws of thermodynamics [28]. Accordingly, it is possible to define the physical volume control limit as the physical area of the investigated system (the fuel cell in this case), and the corresponding equation for energy analysis can simply be defined as the following (Equation 1):

$$Q - W = \Delta H \tag{1}$$

Where; (ΔH) represents enthalpy change, Q is heat and W is work. If there are no irreversible reactions taking place inside a system, the maximum amount of voltage that can be reached with a fuel cell equals the performance and efficiency of the reversible processes in the system, which can be expressed with a Nernst equation. Specifically designed Nernst equations are provided below considering the use cases for the designed cells as part of this study (Eqn. 2).

$$V_{rev} = 1.229 - 8.5 \cdot 10^{-4}(T_{FC} - 298.25) + 4.3085 \cdot 10^{-5} \cdot T_{FC}\left[\ln\left(p_{H_2}\right) + \frac{1}{2}\ln\left(p_{O_2}\right)\right] \tag{2}$$

Where; V_{rev} is the reversible cell voltage and T_{FC} is the cell reaction temperature. In the above equation, hydrogen and oxygen pressures can be determined using the following:

$$p_{H_2} = \frac{1 - x_{H_2O,A}}{1 + (x_A / 2)(1 + \xi_A /(\xi_A - 1))} \cdot P_A \tag{3}$$

$$p_{O_2} = \frac{1 - x_{H_2O,C}}{1 + (x_C / 2)(1 + \xi_C /(\xi_C - 1))} \cdot P_C \tag{4}$$

For equations (3) and (4), p_{H_2} and p_{O_2} hydrogen and oxygen partial pressures, x_{H_2O}, x_A, and x_C denote mole fraction of water, mole fraction of the anode, and for the cathode dry gas, respectively. Anode and cathode stoichiometric constants are denoted by ξ_A ,$\xi_C \xi_C \xi_C$. P_A,P_C are the anode andcathode pressures in atm, respectively.

Actual operational voltages of a given fuel cell can be determined by determining the amount of "irreversibility" first, which are based on the inefficiencies identified in the

system. This amount is then deduced from the total reversible system voltage, as provided in equation 5 below.

$$V_{opr} = V_{rev} - V_{irrev} \tag{5}$$

The irreversibilities of a fuel cell system can be categorized in three main groups as "activation", "ohmic", and "concentration" irreversibilities [29]–[31]. These are represented in the equation below (Equation 6).

$$V_{Irrev} = V_{act} + V_{ohm} + V_{con} \tag{6}$$

"Activation losses" occur in low reaction rates, which are teoretically expressed and determined using equations 7 and 8 provided below:

$$vact, Anode = \frac{RT_{FC}}{\alpha_A nF} ln\ ln\ \left(\frac{i}{i_0}\right) \tag{7}$$

$$vact, Cathode = \frac{RT_{FC}}{\alpha_C nF} ln\ ln\ \left(\frac{i}{i_0}\right) \tag{8}$$

Where i is current density (A cm^{-2}); i_0 is exchange current density (A cm^{-2}); R is the universal gas constant (J $(kmol\ K)^{-1}$); n is the number electrons involved; F is the Faraday's constant (C $mole^{-1}$); n is number of electron involved α_A and α_C are the empirically determined electron transfer coefficient of the reaction at the electrodes at the anode and cathode.

Certain amount of voltage is expected to be lost, resulting in further inefficiency, due to the electrical resistances of the elements used in the production of the fuel cell. The amount of the voltage lost increases as the density of the current drawn from the system increases. According to the literature [16], [32], this loss can be accounted for using the following equations (eqn. 9-13):

$$v_{ohm} = i\, R_{ohm} \tag{9}$$

$$R_{ohm} = \frac{t_{mem}}{\sigma_{mem}} \tag{10}$$

$$\sigma_{mem} = \left(0.005139\, \lambda_{mem} - 0.00326\right) \times \exp\left[1268\, \frac{1}{303} - \frac{1}{T_{FC}}\right] \tag{11}$$

Membrane humidity is determined from the membrane water activity, a, from the following equation;

$$\lambda_{mem} = \begin{Bmatrix} 0.043 + 17.81a - 39.85a^2 + 39.85a^3\ , \\ 0 < a \le 1 \\ 14 + 1.4(a-1) \\ 1 < a \le 3 \end{Bmatrix} \tag{12}$$

$$a = \frac{x_{H_2O} P}{P_{sat}} \tag{13}$$

Where; σ_{mem} corresponds to the conductivity of the membrane ($1\Omega^{-1}cm^{-1}$), while λ_{mem} corresponds to the amount of water inside the membrane. t_{mem} is membrane thickness, x_{H_2O} denotes the mole fraction of the water. P_{sat} is saturation pressure.

Concentration over-potential is caused by a high rate of reaction due to the fact that the concentration tends to drop sharply, which particularly true for higher current densities. Homogenous distribution of the gas flow is important to reduce or prevent any such potential concentrations drops.

$$v_{conc} = i\left(\beta_1 \frac{i}{i_{max}}\right)^{\beta_2} \tag{14}$$

$$\beta_1 = \begin{cases} if \ \frac{p_{O_2}}{0.1173} + P_{sat} < 2 \\ (7.16 \cdot 10^{-4} T_{FC} - 0.622)(\frac{p_{O_2}}{0.1173} + P_{sat}) + \\ (-1.45 \cdot 10^{-3} T_{FC} + 1.68) \\ else \\ (8.66 \cdot 10^{-5} T_{FC} - 0.068)(\frac{p_{O_2}}{0.1173} + P_{sat}) + \\ (-1.6 \cdot 10^{-4} + 0.54) \end{cases} \tag{15}$$

Equations 14 and 15 have contain constants such as β_1, β_2 and i_{max}, all of which are well-defined by the literature and are resolved using empirical equations. The conditions and assumptions stated in the models are taken from the doctoral thesis [33].

4. Results and Discussion

The present study provides the designs for a total of six different fuel cells and their respective analyzes, all of which were performed with COMSOL Multiphysics software. The following section contains information regarding the results of these analyses and their graphical interpretations.

During the modeling, the total area of active membranes was arranged to be the same for all models, and the channels within the plates were roughly set to be the same size. The primary aim during the design of the plates was the homogeneously fuel distribution over the surface. The models are generated depending on the formations already used in the literature and the formations that seems to be potential.

Voltage levels applied on the designed fuel cells were also kept constant (0.5V-0.9V). Channel widths and heights were kept constant as well to ensure a consistent comparison of parameters at an equal setting. This also had the benefit of resulting in same pressure drops and flow rates for the fuel cells.

The verification of the findings of the study was performed by comparing the results of the simulations with the previous studies, especially Mert et al, 2007-2011 [16], [31] and found that the simulation model is in a good harmony with the model that already verified by experimental studies.

Figure 6 displays 3D models of the designed flow plates. Detailed configuration and properties for each design is provided in detail in its own section below.

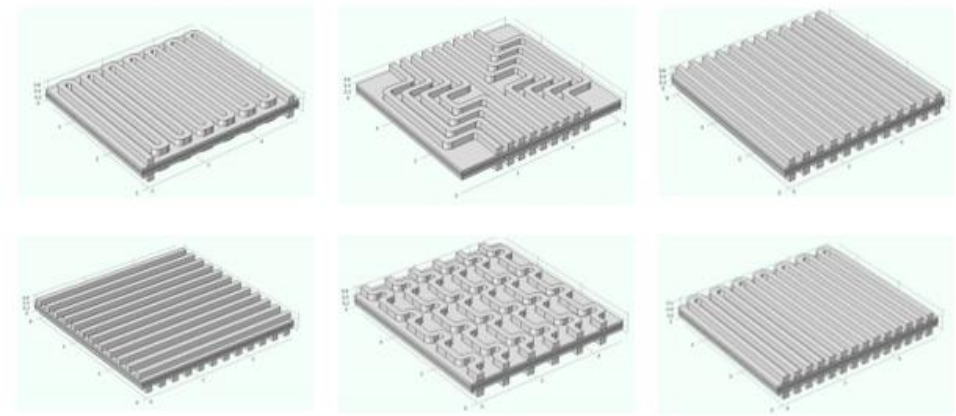

Fig. 6 3D models of the 6 different designs

4.1. Design 1

In the design 1, a model spread over the 13-curve area with a single entrance and exit in the classical S form was selected and examined. Channels with a surface area of 52.98 cm^2 and a volume of 2.661 cm^3 have been completed on anode and cathode plates with a total surface area of 59.62 cm^2 and a total volume of 2.175 cm^3.

The parameters necessary to simulate the fuel cell operation were then configured into the system, and the "3D Mesh" property of the software was used to perform the further studies on the design. The 3D mesh of the model can be seen in Figure 7.. This mesh was the basis for the future analysis.

Fig. 7 3D mesh view of 13 Curve Fuel Cell

The network structure of the designed fuel cell is given in 3D as shown in Figure 7. In the solution network a total of 1.510.434 four-surfaces (Tetrahedral), 53.919 pyramids, 474.059 prisms, 296.911 triangle elements were used, enhanced with corner refinement and boundary layers auxiliary elements. The smallest element size was 0,0034 cm, while the average element size was 0,63 cm.

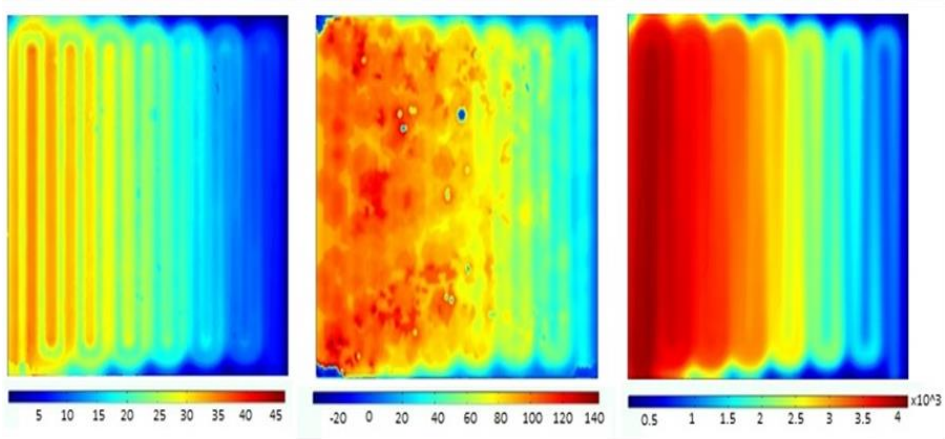

(a) (b) (c)

Fig. 8 2D Membrane Current Density (a) 0,2975 cm (b) 0,3175 cm (c) 0,3375 cm

Depending on the thickness of the membrane in the fuel cell, the current density distribution in the constant working voltage range (0.5 V) is shown in Figure 8. The red color represents high current density, while the blue color represents low current density. The effect of current density on the membrane is shown graphically in the region where the membrane shown in the Figure 8 (a) is 0,2975 cm in the y-axis. In this relatively close formation channel, the effect of the channel on the current density is strikingly visible. As expected, the current density is high in the input zone due to its high reaction rate and decreases gradually towards the output area. In all images of Figure 8, due to the increasing consumption of reactants, the current density decreases gradually along the gas flow direction. Therefore, it is observed that the current density increases as the membrane thickness increases, but it is far from the desired homogeneity.

The effect of the current density on the membrane is shown graphically at the mid-point where the thickness of the membrane shown in the Figure 8 (b) is determined as 0,3175 cm. Depending on the duct design, the distribution of the inlet region is somewhat spread, but an uneven current density and reaction rate are still observed.

The current density distribution is shown in Figure 8 (c). The y axis of the membrane shown in the figure is determined as 0,33375 cm and the effect of current density on the membrane is shown graphically. As seen in the graphs, current density values vary depending on the thickness of the membrane used in the fuel cell.

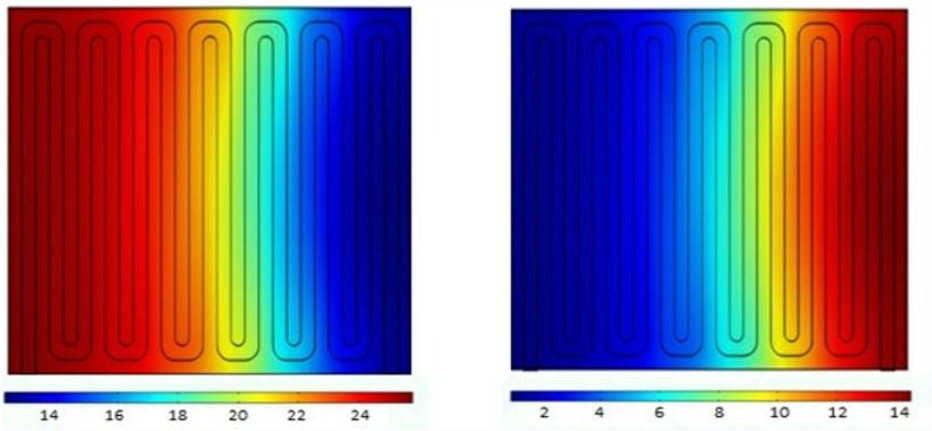

Fig. 9 Distribution of the (a) hydrogen concentration (b) water concentration in the x-y plane of the anode side

The anode reaction that takes place at the system, and the changes on the hydrogen concentration, can be observed in Figure 9 (a). As can be seen, H_2 concentration declines in the +x direction, while the formation of water increases. While hydrogen density is 24 mol/m^3 at the inlet, it decreases to 14 mol/m^3 towards the outlet.

Figure 9 (b) displays the anode reaction and the change in water concentration parameter over the course of the flow channels. The water concentration evidently rises in the + x axis. Considering this information in line with the information from the previous figure, it can be seen that the water formation is almost in parallel with H_2 formation in terms of actual amounts produced. In that regard this system can be considered quite efficient. Concentration graph also shows that the water content increased from 2 mol/m^3 to 14 mol/m^3 during the course of the plate.

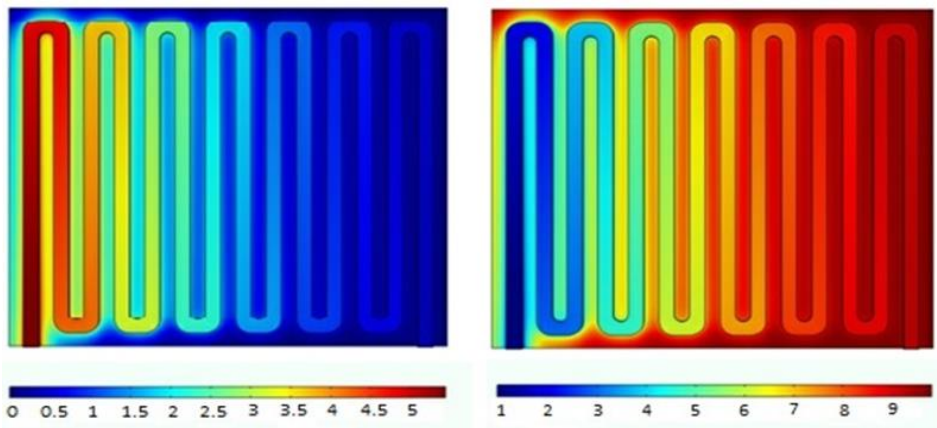

Fig. 10 (a) oxygen concentration and (b) water concentration graphs for the cathode side

Figure 10 (a) displays the change in the oxygen concentration over the course of the plate during the cathode reaction. As is evident, oxygen concentration decreases as the gas flows further, which happens due to the consumption of reactants by electrochemical reactions.

While the oxygen concentration was 5 mol/m^3 at the inlet, it decreased to 0.5 mol/m^3 at the outlet.

Figure 10 (b), on the other hand, displays the change in water concentration over the course of the plate during the cathode reaction. It can be seen here that the water concentration increases towards the later stages of the flow, and the amount of water generated is roughly equal to the amount of O_2 consumed. This is evidence for an efficient system. When looking at the concentration change graph of water, it was observed that it increased from 1 mol/m^3 to 9 mol/m^3.

For the following section, the results will similarly be evaluated for 2D membrane current density and the distribution of the anode and cathode side water concentrations in the x-y plane.

4.2. Design 2

Design 2 is formed as 9 input-output diamond-shaped channel formation. The channels with a surface area of 61.12 cm^2 and a volume of 2.863 cm^3 are designed on anode and cathode plates with a surface area of 69.08 cm^2 and 2.173 volume of cm^3. In the network structure of the flow plate designed by Tetrahedral prisms, 304.527 triangular elements, corner refinement and boundary layers auxiliary elements were also used in the solution using 66.732 pyramids, 587.451. The smallest element size is 0,0039 cm, and the average element size is 0,52 cm.

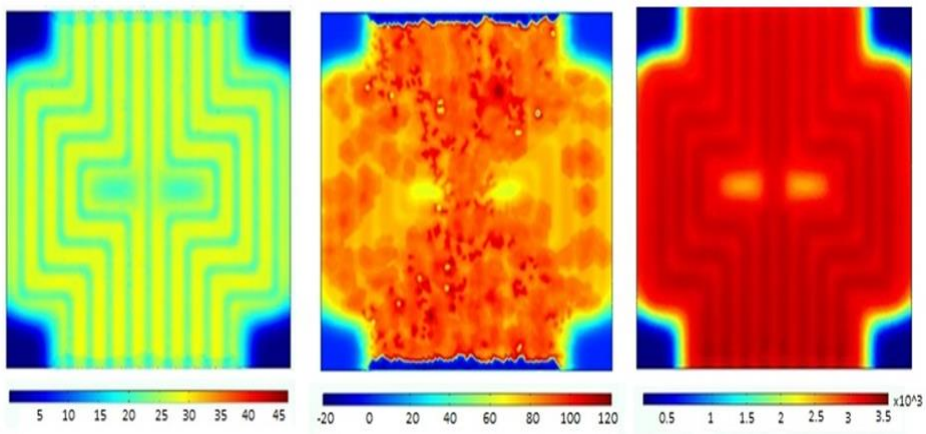

(a) (b) (c)

Fig. 11 2D Membrane Current Density (a) 0,2975 cm (b) 0,3175 cm (c) 0,3375 cm

The current density distribution of the membrane in the fuel cell depending on the y dimension is provided in Figure 11. It is visible that an accumulation occurs in the +Y axis, particularly towards the middle sections. Compared to the first design, this flow plate can be said to have a lower efficiency, mostly caused by the dead zones located at the four corners. The remianing section of the fuel cell system, however, remains at higher rates when compared to the other designs due to the dense channel formation it has. Although it is more homogeneous than Design 1, it shows lower performance due to inefficient areas in the corners.

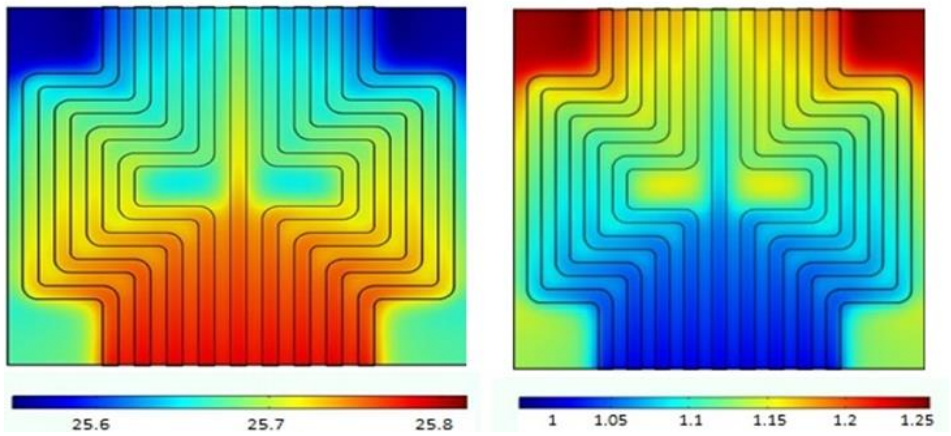

(a) (b)

Fig. 12 Distribution of the (a) hydrogen concentration (b) water concentration in the x-y plane of the anode side.

Figure 12 (a) shows the change of hydrogen concentration in the reaction taking place at constant working voltage (0.55 V) on the anode side. Since hydrogen is consumed during the reaction, it is seen that the hydrogen gradually decreases towards the gas flow direction. While hydrogen density was 25.8 mol/m^3 at the inlet, it decreased to 25.65 mol/m^3 towards the outlet. According to Design 1, it can be said that it is an inefficient design since the use of hydrogen is very low.

Figure 12 (b) shows the change of water concentration in the reaction taking place at constant working voltage (0.55 V) on the anode side. According to the water concentration change graph, it was observed that it increased from 1 mol/m^3 to 1.23 mol/m^3. The water concentration change was very low. So, this design may generally considered to be inefficient.

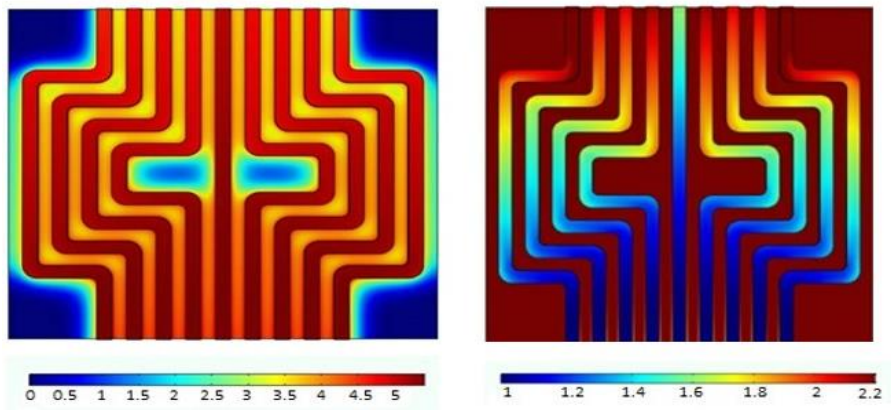

(a) (b)

Fig. 13 Distribution of the (a) oxygen concentration (b) water concentration in the x-y plane of the cathode side

The concentration change of the reaction that took place in the cathode half reaction is shown in Figure 13(a). As with the anode half reaction, it was observed that the concentration change was low in the cathode half reaction. It can be said that the geometry of the flow plate is not suitable for efficiency. Oxygen was 5 mol/m^3 at the inlet but decreased to 4.5 mol/m^3 at the outlet. Similar to the anode side, small changes have also occurred on the cathode side. Thus, it was seen that design 2 was quite inefficient compared to Design 1.

Figure 13 (b) shows the amount of water generation in relation with the O_2 amount on the cathode side. While water is also generated in the cathode side of the fuel cell, the amount of generated is comparatively small. According to the water concentration change graph, it was observed that it increased from 1 mol/m^3 to 2.2 mol/m^3, which amounts to a minor amount of change. This small amount is indicative of adverse effects in action on the plate, as further evidenced by formation of the undesired water. This particular flow plate design, therefore, can be said to have a low overall efficiency.

4.3. Design 3

With 12 straight inputs and outputs Design 3 has Channels with a surface area of 58.56 cm^2 and a volume of 2.88 cm^3 are designed on anode and cathode plates with a surface area of 73.8 cm^2 and 2.7 volume of cm^3.

In the network structure of the flow plate there are 1.221.031 four-surface (Tetrahedral), 49.813 pyramids, 447.719 prisms, 284.545 triangle elements, corner refinement and boundary layers auxiliary elements are also used for different flow channels. The smallest element size is 0,0023 cm, while the average element size is selected as 0,50 cm.

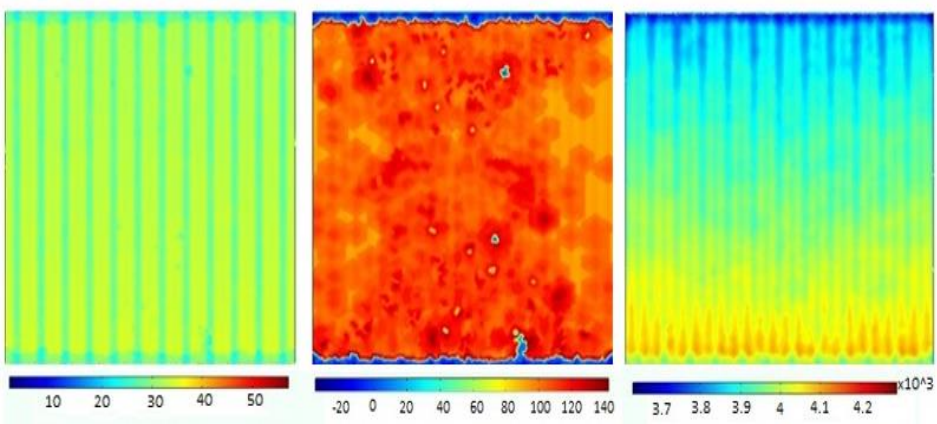

(a) (b) (c)

Fig. 14 2D Membrane Current Density (a) 0,2975 cm (b) 0,3175 cm (c) 0,3375 cm

The current density for the membrane of third design is provided Figure 14 . While the membrane thickness increased, the current density was found to stay homogeneous on all surfaces. Design 3 shows a more homogeneous distribution than Design 1. Since there are no inefficient regions in this design, the design is more positive than the Design 2. It can be said that it is more efficient Designs 1 and 2.

Figure 15 (a) shows the change of hydrogen concentration in the reaction taking place at constant working voltage (0.5 V) on the anode side. While hydrogen density was 25.8 mol/m^3 at the inlet, it decreased to 25.65 mol/m^3 towards the outlet. Although the use of

hydrogen is lower in this design, it can be said that the Design 2 is more efficient because of its wider activity area. Figure 15 (b) shows that water generation increased from 1 mol/m^3 to 1.25 mol/m^3, as can be seen in the water concentration change graph. The water concentration change is very low, but the design can still be considered "efficient" since it's active on all surfaces.

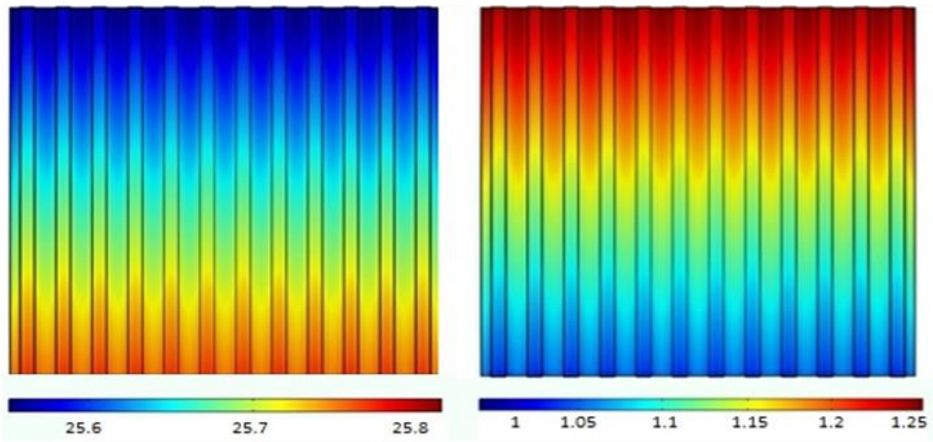

(a) (b)

Fig. 15 Distribution of the (a) hydrogen concentration (b) water concentration in the x-y plane of the anode side.

Oxygen concentration was 3.5 mol/m^3 at the inlet (Figure 16(a)), but decreased to 2.5 mol/m^3 at the outlet. Small changes were found to occur on the cathode side as well as on the anode side. As can be seen in Figure 16 (b), however, the water concentration changes from 3.5 mol/m^3 to 5.5 mol/m^3.

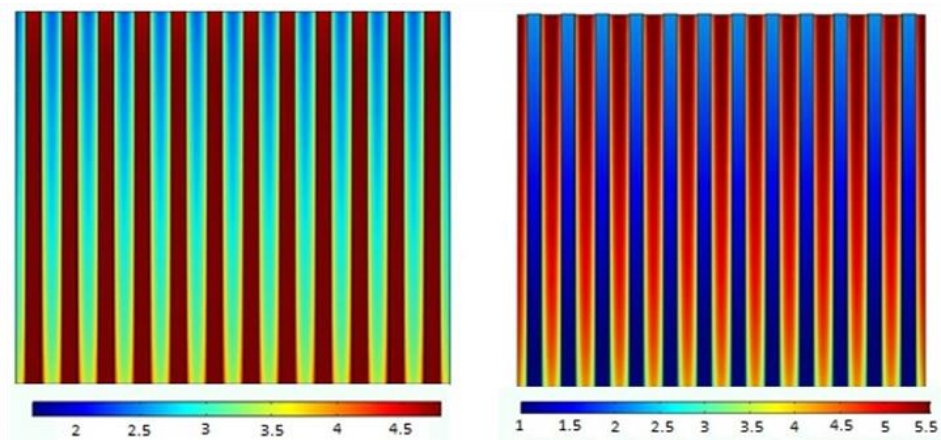

(a) (b)

Fig. 16 Distribution of the (a) oxygen concentration (b) water concentration in the x-y plane of the cathode side.

When the anode and cathode reactant concentrations are examined, the positive effect of multiple inputs can be observed as evidenced in Figure 15 and 16. The reaction is

monitored over a wider active area and at high concentrations. Fuel cell water management is also considered to be more easily applicable in this design.

4.4. Design 4

Design 4 composed of 12 reverse-straight inputs and outputs. Channels with a surface area of 58.56 cm^2 and a volume of 2.88 cm^3 are designed on anode and cathode plates with a surface area of 73.8 cm^2 and 2.7 volume of cm^3. The solution network used 1.187.049 four-surfaces (Tetrahedral), 48.659 pyramids, 429.385 prisms, 276.247 triangular elements, enhanced with corner development and corner layers (Boundary Layers) auxiliary elements for different flow channels. The smallest element size is 0,0023 cm, while the average element size is selected as 0,50 cm.

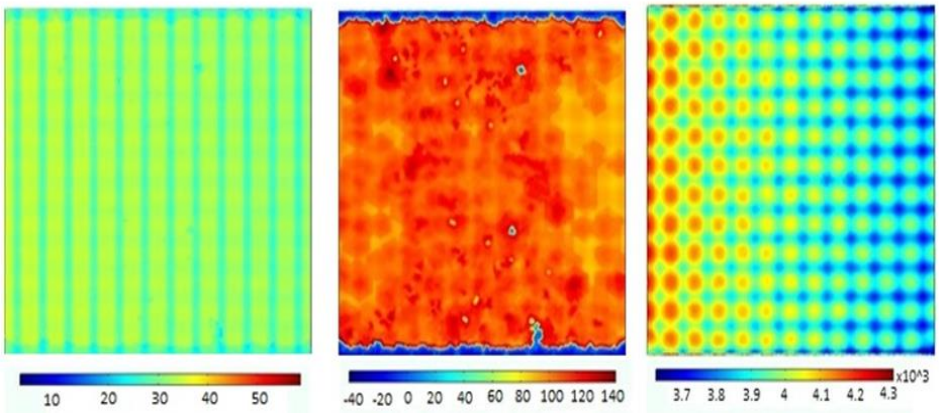

(a) (b) (c)

Fig. 17 2D Membrane Current Density (a) 0,2975 cm (b) 0,3175 cm (c) 0,3375 cm

Examination of the current density in different y-axis sections is shown in Figure 17. The effect of reverse current is clearly seen when compared with Design 3, which is a linear flat design. The current density is scattered across the channels and an interfering distribution is observed. The positive effect of flat channels is still seen in the middle section.

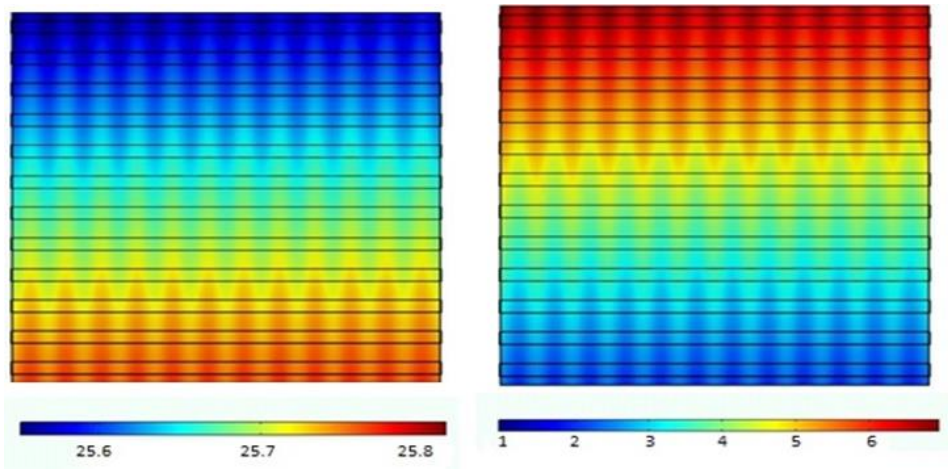

(a) (b)

Fig. 18 Distribution of the (a) hydrogen concentration (b) water concentration in the x-y plane of the anode side.

While hydrogen density was 25.8 mol/m^3 at the inlet, it decreased to 25.6 mol/m^3 towards the outlet. A small amount of change is occurred as seen in Figure 18 (a). Figure 19 (b) shows the distribution of water concentration in the reaction at the cathode interface at constant cell voltage (0.5V). According to the water concentration change graph, the water presence increases from 3 mol/m^3 to 5.5 mol/m^3.

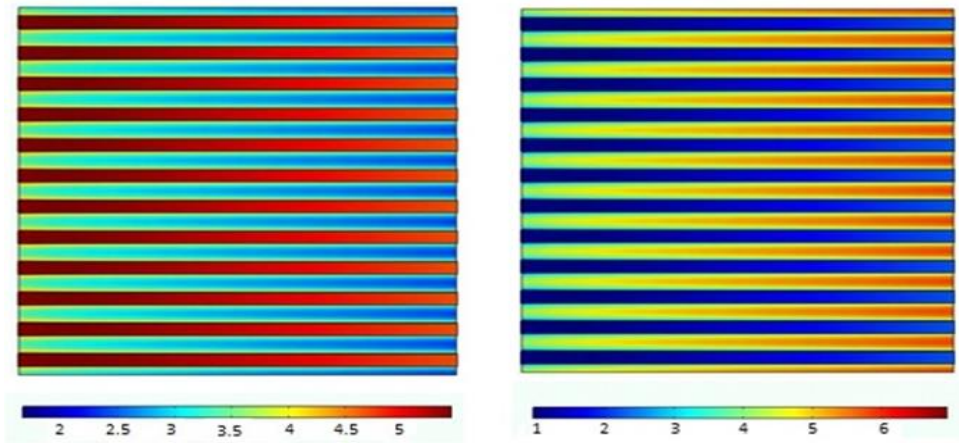

(a) (b)

Fig.19 Distribution of the (a) oxygen concentration (b) water concentration in the x-y plane of the cathode side

Concentration changes along the canals are considered positive with their wide distribution in terms of water management, but changes in oxygen and hydrogen concentrations are considered to be low on the individual canals. Detailed concentration distributions can be examined in Figure 18 and Figure 19. This low drop on concentration

confronts decreases in efficiency and lack of reaction. As the retention time becomes limited the high rate of voltage gradually will increase the efficiency drop.

4.5. Design 5

For sustaining a broader coverage on the cell area a wavy formation is used as presented in some applications on the literature. The wavy fuel cell with 6 inputs and outputs is designed on channels with a surface area of 70.44 cm^2 and a volume of 3.588 cm^3 and anode and cathode plates with a surface area of 100.1 cm^2 and a volume of 3.675 cm^3. There are 3.055.986 four-surface (Tetrahedral), 87.143 pyramids, 1.027193 prisms, 575.956 triangle elements are used, corner refinement and boundary layers auxiliary elements are also used for different flow channels. The smallest element size is 0,0018 cm, while the average element size is 0,51 cm.

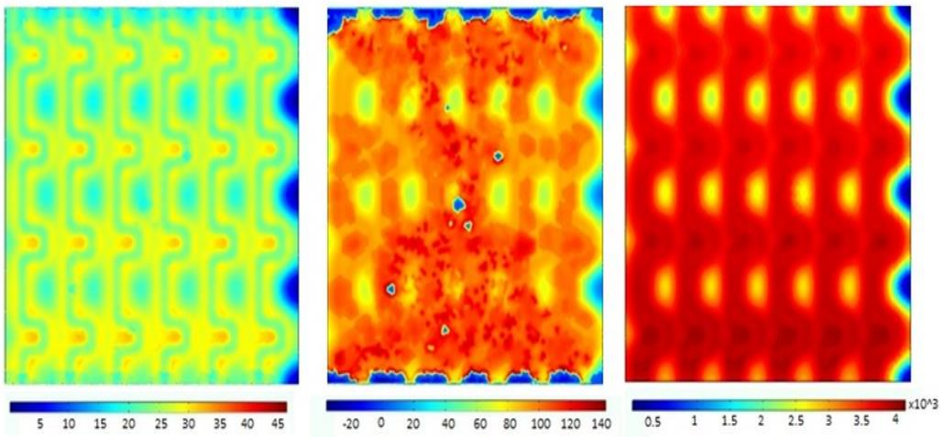

(a) (b) (c)

Fig. 20 2D Membrane Current Density (a) 0,2975 cm (b) 0,3175 cm (c) 0,3375 cm

The effect of the wavy channels used in Design 5 on the current density is shown in Figure 20. The positive effect of multiple inputs and the negative effect of the wavy design on the homogeneous distribution can be observed here. As expected, the current density decreases along the channels and goes down even further in the middle gaps and edges. Inefficient regions arising from the design can also be observed. This design is therefore less homogeneous compared to other designs. That being said, it is also concluded that with a denser structure the distribution can be further optimized in terms of homogeneity. The increased retention time will be another advantage in a denser structure as well.

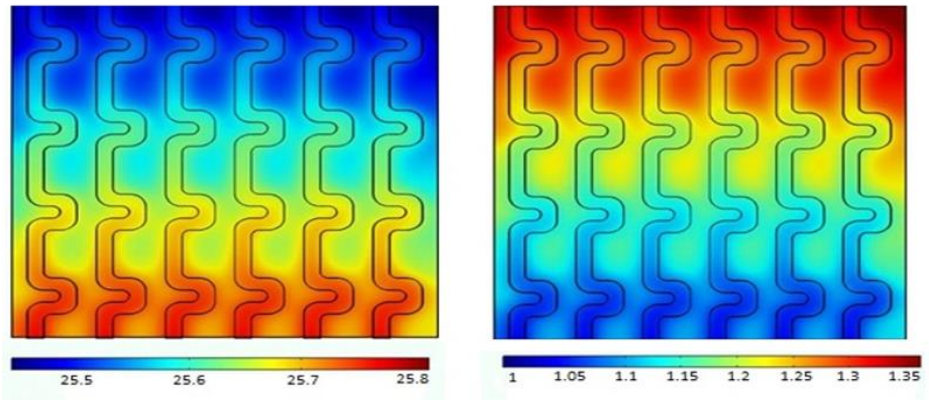

(a) (b)

Figure 21. Distribution of the (a) hydrogen concentration (b) water concentration in the x-y plane of the anode side.

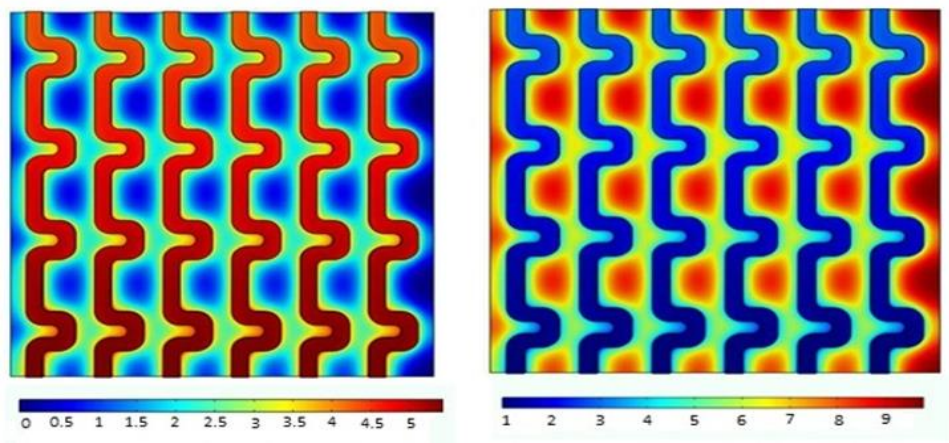

(a) (b)

Fig. 22 Distribution of the (a) oxygen concentration (b) water concentration in the x-y plane of the cathode side.

For Design 5, the concentrations of the components are shown Figures 21 and 22. Hydrogen density was 25.8 mol/m^3 at the inlet, whereas it decreased to 25.5 mol/m^3 towards the outlet. According to the water concentration change graph, it was observed that it increased from 1 mol/m^3 to 1.35 mol/m^3. It is evident that there is a higher reactant distribution than linear channels, and the rapid concentration drops are seen in the entry regions as a result of these. The increase in the retention time of the reactants in the system also enhances the efficiency. The formation, however, still needs to be smoother and denser for the sake of homogeneity and increasing high rates in reaction.

4.6. Design 6

U-shaped fuel cell with 7 inputs and outputs, the channels with a surface area of 61.22 cm^2 and a volume of 3.064 cm^3 are designed on anode and cathode plates with a surface area

of 63.68 cm^2 and a volume of 2.325 cm^3. In the solution network using 1.748.034 four-surface (Tetrahedral), 62.533 pyramids, 553.700 prisms, 345.402 triangle elements, corner refinement and boundary layers auxiliary elements are also used for different flow channels. The smallest element size is 0,0018 cm, while the average element size is 0,52 cm.

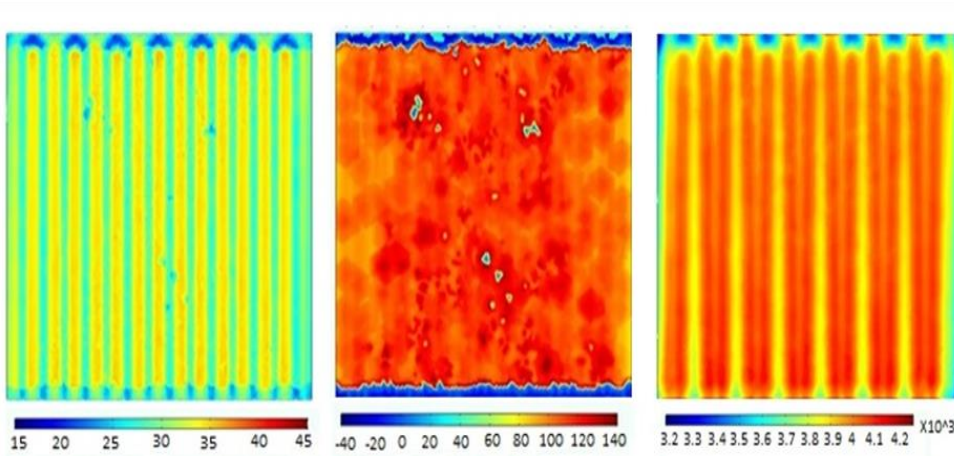

(a) (b) (c)

Fig. 23 2D Membrane Current Density (a) 0,2975 cm (b) 0,3175 cm (c) 0,3375 cm

The current densities of this design, with multiple inlets and outlets which extend the length of the channel with its spiral structure and cover the active area to the maximum, are shown in Figure 23. As a result, a dominant homogeneous structure appears where the majority of the active area is used. Since the canal design covers the entire surface area, it has a lower amount of inefficient zones.

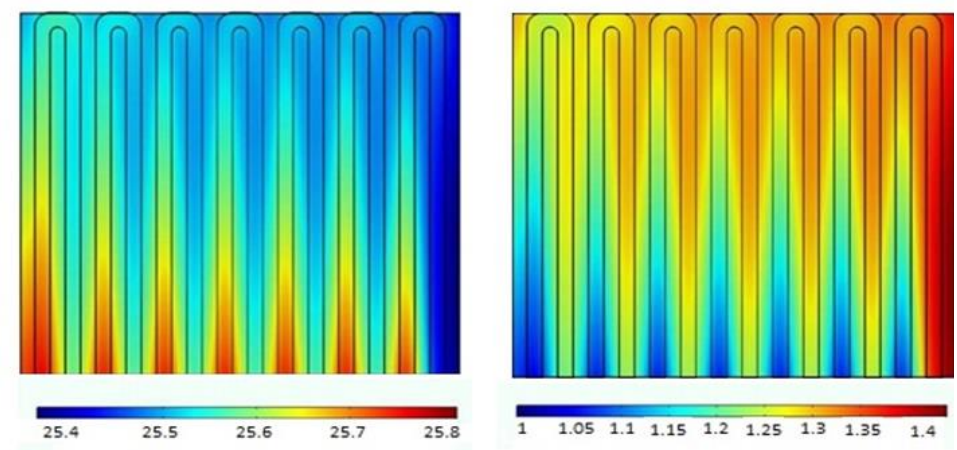

(a) (b)

Fig. 24 Distribution of the (a) hydrogen concentration (b) water concentration in the x-y plane of the anode side

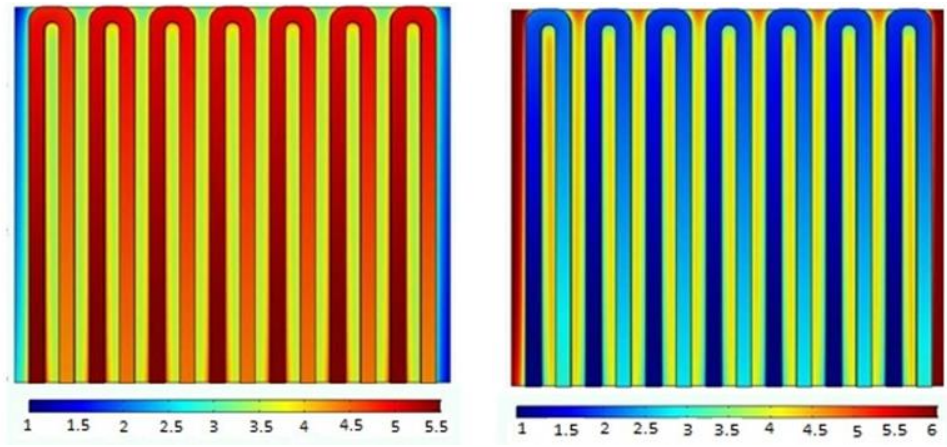

(a) (b)

Fig. 25 Distribution of the (a) oxygen concentration (b) water concentration in the x-y plane of the cathode side

One of the positive features of Design 6 is that it facilitates water management for the fuel cell system. According to Figure 24 and Figure 25, the multi-inlet-outlet channel design prevents excessive drop in concentrations. Accordingly, the hydrogen concentration was 25.8 mol/m^3 at the inlet, but it decreased to 25.4 mol/m^3, due to the relatively long channels providing adequate distribution of the reactants. Oxygen content was 5.5 mol/m^3 at the inlet, but decreased to 4.3 mol/m^3 at the outlet. From water concentration point of view, it was observed that it increased from 1 mol/m^3 to 1.35 mol/m^3 in the anode, whereas it increased from 1 mol/m^3 to 3 mol/m^3 in cathode side (Figure 25-b)

5. Conclusions

Today, due to the increase in environmental pollution, scientists have turned to clean energy. It has been scientifically proven that environmental pollution is mostly caused by vehicles using fossil fuels. For this reason, fuel cell vehicles have come to the fore instead of internal combustion engine vehicles. Fuel cells are highly preferred in vehicles due to their low fuel supply and long driving distance, as well as being environmentally friendly. However, optimum temperature and sufficient humidity must be provided for adequate efficiency from fuel cells. Therefore fuel cells must be well designed.

The present study investigated different flow channel layouts modeled using COMSOL Multiphysics program. A series of performance analyses were performed on these flow plates to determine their current densities, changes in hydrogen and oxygen contents, and overall efficiencies.

When the surface area of a given flow plate is used homogenously, the potential damage due to focal degenerations or breakdowns will be minimized. These focal degenerations occur as a result of high reaction rates in particular locations and the homogeneity of the reaction over the course of the reactant flow helps prevent them from taking place, making it very important in terms of overall efficiency and performance. From this perspective, multiple input fuel cell designs were found to help disperse the fuel on the membrane more equally, which in turn help achieve higher efficiencies. Similarly, cross-flow channels were with relatively shorter lengths were found to lead to more positive results compared to

their longer or parallel flow counterparts. As the cross-flow channels get longer, however, they begin to have negative effects.

We are hopeful that the findings of this study will present a useful source for those who are interested in fuel cell designs, particularly for those with vehicular use in mind. The modeling and simulation method used in the study reduces the time needed for the design stage and can reduce the number of experimental tests in search for the optimal flow plate design.

Acknowledgement

The authors would like to acknowledge the financial support of the Scientific Research Projects Fund of Yüzüncü Yıl University (YYÜ-BAP- 2015-MİM-B120) for the study, along with the Scientific and Technological Research Council of Turkey (TÜBİTAK-MAG-115M741). Also, author Ceyda KÖK is sponsored via a fellowship from the YOK 100/2000 Electric and Hybrid Vehicles Doctorate Program.

References

[1] Hilton Holloway. Japan pushes hydrogen infrastructure | Autocar, Autocar, 2011.
[2] IEA. CO2 EMISSIONS FROM FUEL COMBUSTION Highlights, Iea, 2015.
[3] Giorgi L. Fuel Cells: Technologies and Applications. Open Fuel Cells J, 2013. https://doi.org/10.2174/1875932720130719001
[4] Offer G, James G. Comparative analysis of battery electric, hydrogen fuel cell and hybrid vehicles in a future sustainable road transport system. Energy policy, 2010, 38.1: 24-29 https://doi.org/10.1016/j.enpol.2009.08.040
[5] Choi H, Shin J, Woo JR. Effect of electricity generation mix on battery electric vehicle adoption and its environmental impact, Energy Policy, 2018. https://doi.org/10.1016/j.enpol.2018.06.013
[6] IEA. World Energy Outlook, Iea, 2014.
[7] Kopp M, Coleman D, Stiller C, Scheffer K, Aichinger J, Scheppat B. Energiepark Mainz: Technical and economic analysis of the worldwide largest Power-to-Gas plant with PEM electrolysis. International Journal of Hydrogen Energy, 2017; 42(19), 13311-13320. https://doi.org/10.1016/j.ijhydene.2016.12.145
[8] Fahim KH, MAlfayydh EA. Effect of Geometric Design of the Flow Fields Plat on the Performance of A PEM Fuel Cell: A Review. Int. J. Sci. Eng. Res., 2017.
[9] Pal V, Karthikeyan P, Anand R. Performance Enhancement of the Proton Exchange Membrane Fuel Cell Using Pin Type Flow Channel with Porous Inserts. J. Power Energy Eng., 2015. https://doi.org/10.4236/jpee.2015.35001
[10] Edupuganti V. An Investigation of the Impact of the Proton Exchange Membrane Fuel Cell Flow Field Plate Geometry and Design Using Computational Fluid Dynamic Modeling and Simulation. 2012; 27.
[11] Velisala V, Srinivasulu GN. Computational fluid dynamics study of 3-pass serpentine flow field configuration on proton exchange membrane fuel cell performance. Int. J. Ambient Energy, 2020.
[12] Shen J, Tu Z, Chan SH. Evaluation criterion of different flow field patterns in a proton exchange membrane fuel cell. Energy Conversion and Management, 2020; 213, 112841. https://doi.org/10.1016/j.enconman.2020.112841
[13] Shen J, Tu Z, Chan SH. Performance enhancement in a proton exchange membrane fuel cell with a novel 3D flow field. Applied Thermal Engineering, 2020;164, 114464. https://doi.org/10.1016/j.applthermaleng.2019.114464
[14] Badduri SR, Srinivasulu GN, Rao SS. Influence of bio-inspired flow channel designs on the performance of a PEM fuel cell. Chinese Journal of Chemical Engineering, 2020; 28(3), 824-831. https://doi.org/10.1016/j.cjche.2019.07.010

[15] Liao Z, Wei L, Dafalla AM, Guo J, Jiang F. Analysis of the impact of flow field arrangement on the performance of PEMFC with zigzag-shaped channels. International Journal of Heat and Mass Transfer, 2021;181, 121900.
[16] Mert SO, Özçelik Z, Özçelik Y, Dinçer I. Multi-objective optimization of a vehicular PEM fuel cell system. Applied Thermal Engineering, 2011; 31(13), 2171-2176. https://doi.org/10.1016/j.applthermaleng.2011.04.031
[17] EG&G Technical Services, I. EG&G Technical Services. Fuel Cell Technology-Handbook, 7th Edition. U.S. Department of Energy, 2004.
[18] Hoogers G. Fuel Cell Technology - Handbook. CRC Press, 2003. https://doi.org/10.1201/9781420041552
[19] Andújar JM, Segura F. Fuel cells: History and updating. A walk along two centuries. Renewable and sustainable energy reviews, 2009; 13(9), 2309-2322. https://doi.org/10.1016/j.rser.2009.03.015
[20] Larminie J, Dicks A, Mcdonald M. Fuel cell systems explained. Chichester, UK: J. Wiley, 2003. https://doi.org/10.1002/9781118878330
[21] Barbir F. PEM Fuel Cells-Theory and Practice. Elsevier Academic Press, 2005.
[22] Kirubakaran, Jain S, Nema RK. The PEM Fuel Cell System with DC/DC Boost Converter: Design, Modeling and Simulation. Int. J. Recent Trends Eng., 2009.
[23] O'Hayre R, Colella W, Prinz FB. Fuel Cell Fundamentals. 2016. https://doi.org/10.1002/9781119191766
[24] Emadi A, Williamson SS. Fuel cell vehicles: opportunities and challenges. IEEE Power Engineering Society General Meeting, 2004; 1640-1645
[25] Dickinson EJ, Ekström H, Fontes E. COMSOL Multiphysics®: Finite element software for electrochemical analysis. A mini-review. Electrochemistry communications, 2014;40, 71-74. https://doi.org/10.1016/j.elecom.2013.12.020
[26] Comsol A. Comsol Multiphysics User's Guide. 2010.
[27] Vick JA. Multiphysics Simulation. IEEE Spectr., 2013.
[28] Wang L, Husar A, Zhou T, Liu H. A parametric study of PEM fuel cell performances. International journal of hydrogen energy, 2003; 28(11), 1263-1272. https://doi.org/10.1016/S0360-3199(02)00284-7
[29] Hussain MM, Baschuk JJ, Li X, Dincer I. Thermodynamic analysis of a PEM fuel cell power system. International journal of thermal sciences, 2005; 44(9), 903-911. https://doi.org/10.1016/j.ijthermalsci.2005.02.009
[30] Kazim A. Exergy analysis of a PEM fuel cell at variable operating conditions. Energy conversion and management, 2004; 45(11-12), 1949-1961. https://doi.org/10.1016/j.enconman.2003.09.030
[31] Mert SO, Dincer I, Ozcelik Z. Exergoeconomic analysis of a vehicular PEM fuel cell system. Journal of Power Sources, 2007; 165(1), 244-252. https://doi.org/10.1016/j.jpowsour.2006.12.002
[32] Midilli A, Dincer I. Exergetic performance analysis of a PEM fuel cell. Int. J. Energy, 2006; 307-321. https://doi.org/10.1002/er.1150
[33] Mert SO. (2012). Exergetıc based multı-objectıve optımızatıon of selected fuel cell systems. Ph.D. Dissertation, Ege University, Turkey.